Multi-dimensional Limiting Strategy for Robust, Accurate and Efficient Computations of Compressible Flows on Unstructured Meshes

Jin Seok Park, Sung-Hwan Yoon, Chongam Kim*

* School of Mechanical and Aerospace Engineering, Seoul National University, Seoul, Korea
(Tel : +82-2-880-1915; E-mail: chongam@snu.ac.kr)

Abstract: The present paper deals with the accurate and robust limiting procedure for the multi-dimensional flow analysis on unstructured meshes. The multi-dimensional limiting process (MLP) which was successfully proposed on structured grid system is extended to unstructured meshes. Based on MUSCL-type framework on unstructured meshes, the new slope limiter is devised to satisfy the MLP condition, which is quite effective to regulate the unwanted oscillations, especially on multiple dimensions. Considering the neighborhood based on the vertex of the cell, as well as the edge, this limiting strategy captures the multi-dimensional flow features very accurately with the proper stencils. From the various numerical results, these desirable characteristics of the proposed limiting strategy are clearly shown.

Keywords: Multi-dimensional limiting process, MLP condition, MUSCL-type, Unstructured meshes

1. INTRODUCTION

The rapid development of computational technology makes it possible to analyze the complex flow structure numerically. Though the most of mathematical theory for Euler and Navier-Stokes equations is developed in simple one dimensional space, it is readily extended to analyzing multi-dimensional flow and solving the flow pattern around intricate boundary. As a consequence the several researches have been carried out to handle a complex geometry. Among them, unstructured meshes technique is one of the most successful approaches due to its flexible tessellation.

To resolve the complex flow accurately and efficiently, the robust high resolution scheme, without occurring spurious oscillations, is essential. However, most oscillation-free schemes are mainly based on the mathematical analysis of one-dimensional convection equation, and applied to systems of equations with the help of some linearization step. Especially, the TVD condition[1,2], which is a fundamental idea of restricting these oscillations, is inadequate on multiple dimensions maintaining high order accuracy[3]. Even though these schemes can be applicable on structured meshes by dimensional splitting manner and it may work successfully in many cases, it is often insufficient or almost impossible to control oscillations near shock discontinuity in multi-dimensional flow. Moreover, adapting these schemes directly on unstructured meshes seems to be almost impossible. In this respect, exploring an oscillation control method for multi-dimensional applications is obviously needed, especially on unstructured meshes due to its geometric complexity.

In order to find out a suitable criterion for oscillation control in multiple dimensions, the one-dimensional monotonic condition was extended to multi-dimensional flows and our group successfully formulated the multi-dimensional limiting process (MLP), which showed enhanced accuracy and convergence for numerous inviscid and viscous computations on structured meshes[4,5]. Thus, it is expected that this strategy can be applied on unstructured meshes with some modifications.

The aim of the present paper is devising the new limiting process on unstructured meshes extending the MLP on structured meshes. At first, the MUSCL-type framework on unstructured meshes is briefly mentioned on section 2. Then, the MLP on structured meshes is summarized and unstructured version of MLP is introduced on section 3. In Section 4, numerical test cases are presented to verify the performance of present method. Finally, conclusion is given in Section 5.

2. FINITE VOLUME METHODS ON UNSTURCTURED MESHES

2.1 Framework of MUSCL-type approach

Consider the multi-dimensional hyperbolic conservation laws,

$$\mathbf{Q}_t + \mathbf{F}(\mathbf{Q})_x = \mathbf{0} , \qquad (1)$$

where $\mathbf{Q}$ is the state variable vector and $\mathbf{F}$ is the flux function vector.

In order to resolve discontinuities which occur on the solution of a hyperbolic system, finite volume method is appropriate. There are two approaches of finite volume method on unstructured meshes: one is cell-centered approach whose control volume is a triangle generated by mesh, the other is cell-vertex approach whose control volume is from median dual. It is controversial that which approach is better for accurate and efficient calculation. Regarding that one of motivation of this research is extension of MLP on structured meshes, the cell-centered approach, which is more natural extension of structured meshes, is applied. With the numerical flux function, the semi-discretized form of Eq. (1) for each component on the control volume T_j is written as follows.

$$\left|T_j\right|\frac{\partial \overline{q}_j}{\partial t} + \sum_{e_{jk} \in T_j} h\left(\overline{q}_{jk}, \overline{q}_{kj}\right)\left|e_{jk}\right| = \mathbf{0} , \qquad (2)$$

where $\overline{q}$ denotes the component of the cell-averaged value, $\overline{q}_{jk}$ is the cell interface state value from the cell T_j to the cell T_k and $\left|T_j\right|$ is the area of the cell T_j. e_{jk} denotes the edge between the cell T_j and the cell T_k and $\left|e_{jk}\right|$ is the length of this edge. $h(q_L, q_R)$ is the numerical flux function.

On Godunov methods, q_L and q_R are cell-averaged values, which assume piecewise constant distribution, but it only guarantees first order spatial accuracy. In order to obtain higher order accurate solution on unstructured meshes, the MUSCL-type framework is introduced. This extends the one dimensional slope limiter, so the value in a cell is assumed to be linearly distributed. For each component, the distribution on the cell is reconstructed as follows.
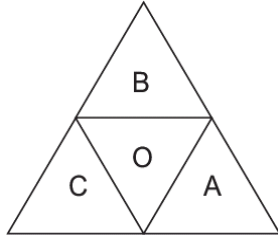
Fig. 1 The neighborhood of the cell T_O .

$$q_j(x,y) = \overline{q}_j + \phi \nabla \overline{q}_j \cdot \mathbf{r} , \qquad (3)$$

where $\nabla \overline{q}_j$ is the gradient of the component on the cell T_j and ϕ is a slope limiter. The cell interface values are calculated by this formula and the second order accurate solution can be obtained.

There are various schemes based on MUSCL-type approach, but the key differences are the gradient calculation and the limiter. The following subsection explains the first part of this framework, linear reconstruction, and then new limiting process is dealt on next section.

2.2 Methods of linear reconstruction

In the one dimensional MUSCL approach, the slope is easily calculated by simple difference formulas. However, due to the geometric complexity of grid system, it is impossible to apply above approaches, thus the linear reconstruction approach is required using neighboring cell values.

The easiest method of linear reconstruction is the simple gradients operator using three cell-averaged values among the cell and its neighborhood[6,7]. Though this method needs little computational cost, it is not clear to choose the appropriate cell-averaged values for operation among the neighborhood (See Fig. 1). Moreover the operation is not robust, especially on a stretched triangular element and it also does not give the accurate gradient. As a consequence, the more accurate and robust methods are required.

One of such method is the least-square reconstruction, which gives the accurate fitting of the gradient using the value of the cell and those of its neighborhood. For the simple triangular mesh, the gradient is estimated by applying Eq. (3) to the neighborhood of the given cell.

$$[\mathbf{L}_1 \ \mathbf{L}_2] \nabla \overline{q}_j = \mathbf{f} , \qquad (4)$$

where $\mathbf{L}_1 = [\Delta x_{OA} \ \Delta x_{OB} \ \Delta x_{OC}]^T$, $\mathbf{L}_2 = [\Delta y_{OA} \ \Delta y_{OB} \ \Delta y_{OC}]^T$ and $\mathbf{f} = [\overline{q}_A - \overline{q}_O \ \overline{q}_A - \overline{q}_O \ \overline{q}_A - \overline{q}_O]^T$. The above matrix is over-determined system so least square fitting technique gives appropriates estimation value of the gradient.

$$\nabla \overline{q}_j = \frac{1}{l_{11}l_{22} - l_{12}^2} \begin{bmatrix} l_{22}(\mathbf{L}_1 \cdot \mathbf{f}) - l_{12}(\mathbf{L}_2 \cdot \mathbf{f}) \\ l_{11}(\mathbf{L}_2 \cdot \mathbf{f}) - l_{12}(\mathbf{L}_1 \cdot \mathbf{f}) \end{bmatrix} , \qquad (5)$$

where $l_{ij} = \mathbf{L}_i \cdot \mathbf{L}_j$. Although this method requires the expensive computational costs, it is flexible to the shape of mesh and easy to extend quadratic or higher order schemes by estimating higher order derivatives. Due to these advantages, the gradient is calculated by least-square reconstruction in this research.

3. MULTI-DIMENSIONAL LIMITING PROCESS ON UNSTRUCTURED MESHES

3.1 Review of MLP on structured meshes

The Godunov approach is usually handled by decoupling interpolation stage and evolution stage. Without modifying the evolution stage, where the local Riemann problem is solved, the piecewise linear or quadratic distribution is applied on interpolation stage to obtain high resolution. One of the most successful ways of this is the MUSCL approach, referred as a second order upwind schemes by applying the piecewise linear distribution.

In order to control oscillatory behavior on one dimension, MUSCL approach with TVD limiter is commonly used. With the symmetric TVD limiter, the cell interface values can be obtained by following simple formula.

$$q_{i+1/2}^L = \overline{q}_i + 0.5\phi(r_L)\Delta\overline{q}_{i-1/2} , \quad q_{i+1/2}^R = \overline{q}_i - 0.5\phi(r_R)\Delta\overline{q}_{i+3/2} \quad (6)$$

where r_L and r_R are the ratios of the slope by neighboring cells, which are defined by $\Delta\overline{q}_{i+1/2} = \overline{q}_{i+1} - \overline{q}_i$, $r_L = \Delta\overline{q}_{i+1/2} / \Delta\overline{q}_{i-1/2}$ and $r_R = \Delta\overline{q}_{i+1/2} / \Delta\overline{q}_{i+3/2}$. The limiter $\phi(r)$ satisfies the symmetric condition of $\phi(r) = r\phi(1/r)$.

One-dimensional limiting condition using the TVD constraint yields the following TVD zone[2] is written as follows.

$$0 \le \phi(r) \le \min(2, 2r) , \qquad (7)$$

With this condition, the one dimensional monotonic distribution can be expressed.

$$\overline{q}_{i-1} \le \overline{q}_i \le \overline{q}_{i+1} , \qquad (8)$$

Though the TVD condition is quite effective to restrict the spurious on oscillations one dimensional space, it does not guarantee monotonic solution on multi-dimensional space. In order to prevent these oscillations, there are several attempts to make multi-dimensional monotonic condition. Among them, MLP is one of the successful ways to regulate these oscillations across a discontinuity in multiple dimensions. Extending from the monotonic distribution of TVD condition Eq. (8), the MLP condition restricts the value at the cell vertex, where the each directional variation is multi-dimensionally summed.

$$\overline{q}_{neighbor}^{min} \le \overline{q}_{vertex} \le \overline{q}_{neighbor}^{min} , \qquad (9)$$

This condition can be readily implemented within TVD-MUSCL framework by adopting variable limiting region. Thus, limiting region of MLP condition can be written as follows.

$$0 \le \phi(r) \le \min(\alpha, \alpha r) , \qquad (10)$$

where α is the multi-dimensional restriction coefficient which determines the baseline limiting region. From the MLP condition, the value of α is obtained by following formula.

$$\alpha = \left| \frac{2\max(1, r_x)}{(1 + r_{xy})\Delta\overline{q}_{i+1/2}} \right| \min\left[\left|\overline{q}^{max} - \overline{q}_{i,j}\right|, \left|\overline{q}^{min} - \overline{q}_{i,j}\right| \right] , \qquad (11)$$

Fig. 2 Baseline MLP region.

Fig. 3 The neighborhood of the cell T_j.
(Shaded region: the group of cells sharing vertex A)

where $r_x = \Delta\overline{q}_{i+1/2,j} / \Delta\overline{q}_{i-1/2,j}$ and $r_{xy} = \Delta\overline{q}^y_{i+k1,j} / \Delta\overline{q}^x_{i+k2,j}$ with $k1, k2 = \pm 1$. While the TVD region is fixed, the MLP limiting region is varying according to the multi-dimensional distribution of property (See Fig. 2).

3.2 MLP condition on unstructured meshes

Referring the successful result of MLP on structured meshes, it is expected that MLP can easily extended on unstructured meshes. However, there are some difficulties for the direct extension of MLP to unstructured meshes. MLP on structured meshes depend the TVD-MUSCL framework, which limits the cell interface values by dimensional splitting manner, and MLP condition, which is essential constraint to remove spurious oscillation by limiting cell vertex values. Because there is no unique base direction for each triangular cell on unstructured meshes, it is unreasonable to obtain directional variations and to limit these variations using cell interface values. In addition, the TVD condition does not guarantee the monotonicity on multiple dimensions and degrade accuracy to the order of one[3]. To cope with these multi-dimensional natures of unstructured grids, the interpolation stage of Godunov approach should be modified, such as MUSCL-type framework on unstructured meshes. Moreover, the other criterion for the monotonicity on multiple dimensions is required to circumvent the limitation of TVD condition.

With the notion of MLP condition of structured grids, the maximum and minimum values at the boundary of a cell should be investigated to prevent spurious oscillations. On MUSCL-type framework of unstructured grids, these are occurred on the vertex of the cell, thus the value at each vertex should be limited by proper method. Comparing to other limiting approaches, MLP condition restricts the value at the vertex, considering the distribution around the vertex itself. Thus, it is reasonable to applying MLP condition Eq. (9) to MUSCL-type framework. Thus, the multi-dimensional slope limiter is bounded by this condition.

$$\frac{\overline{q}^{min}_{neighbor} - \overline{q}}{\nabla q \cdot \mathbf{r}_{vertex}} \le \phi \le \frac{\overline{q}^{max}_{neighbor} - \overline{q}}{\nabla q \cdot \mathbf{r}_{vertex}}, \tag{12}$$

The effectiveness of MLP condition is supported by the maximum principle, which is a complementary condition ensuring the monotonicity on multiple dimensions. It is summarized by following theorem.
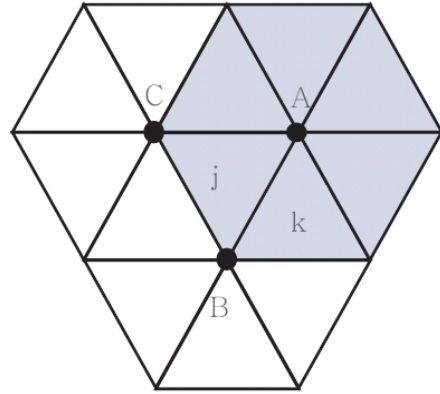
Theorem1. *The fully discrete finite volume scheme of hyperbolic conservation laws with Lipschitz continuous flux function and linear reconstruction exhibit the maximum principle,*

$$\overline{q}^{LB}_j \le \overline{q}_j \le \overline{q}^{UB}_j, \tag{13}$$

if linear reconstruction satisfies the MLP condition under proper CFL restriction. The q^{LB}_j and q^{UB}_j are the lower and upper bound of cell-averaged values among the neighborhood of the cell T_j, which shares at least a common point on this cell. (See Fig. 3)

Proof) Let's denotes $\hat{q}_{v_i,j}$ as the estimated value at the vertex v_i on the cell T_j. From the MLP condition, a value at the vertex satisfies following formula.

$$\hat{q}^{min}_{v_i} \le \hat{q}_{v_i,j} \le \hat{q}^{max}_{v_i}, \tag{14}$$

where $\hat{q}^{min}_{v_i}$ and $\hat{q}^{max}_{v_i}$ are the minimum and maximum values of solution cell averages among the cells which share the vertex v_i. With this definition, the lower and upper bound values of the cell T_j can be rewritten as follows.

$$\overline{q}^{LB}_j = \min_{v_i \in T_j}\left(\hat{q}^{min}_{v_i}\right), \quad \overline{q}^{UB}_j = \max_{v_i \in T_j}\left(\hat{q}^{max}_{v_i}\right). \tag{15}$$

Due to the linear reconstruction, the cell interface values are the linear combination of the values at the vertex.

$$\overline{q}_{jk} = \xi\hat{q}_{v_1,j} + (1-\xi)\hat{q}_{v_2,k}, \quad 0 \le \xi \le 1 \tag{16}$$

$$\overline{q}_{kj} = \zeta\hat{q}_{v_1,k} + (1-\zeta)\hat{q}_{v_2,k}, \quad 0 \le \zeta \le 1 \tag{17}$$

With Eqs. (14)~(17), the interface values are bounded as follows.

$$\overline{q}^{LB}_j \le \overline{q}_{jk}, \overline{q}_{kj} \le \overline{q}^{UB}_j, \tag{18}$$
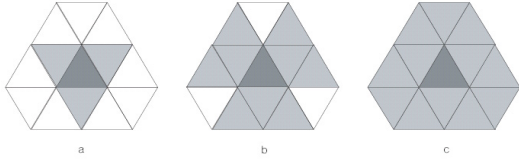
Fig. 4 The comparison stencil for the maximum principle: (a) Maximum principle region by M. E. Hubbard, (b) Barth's limiter and (c) MLP-u.

Apply this inequality to Eq. (2), thus the following relation can be obtained.

$$\frac{\partial \overline{q}_j}{\partial t} \leq -\frac{1}{|T_j|} \sum_{e_{jk} \in T_j} h(\overline{q}_{jk}, \overline{q}_j^{UB})|e_{jk}|$$
$$= -\frac{1}{|T_j|} \sum_{e_{jk} \in T_j} \left[h(\overline{q}_{jk}, \overline{q}_j^{UB}) - h(\overline{q}_{jk}, \overline{q}_{jk}) \right]|e_{jk}|$$
$$= -\frac{1}{|T_j|} \sum_k \frac{\partial h}{\partial q}(\overline{q}_{jk}, \xi)(\overline{q}_j^{UB} - \overline{q}_{jk})|e_{jk}|$$
$$\leq \frac{L_j}{|T_j|} \sup \left| \frac{\partial h}{\partial q} \left(\min_k(\overline{q}_{jk}), \xi \right) \right| (\overline{q}_j^{UB} - \overline{q}_{jk}), \quad (19)$$

where L_j is the diameter of the cell T_j.

With the similar approach, we also obtain another inequality.

$$\frac{\partial \overline{q}_j}{\partial t} \geq \frac{L_j}{|T_j|} \sup \left| \frac{\partial h}{\partial q} \left(\max_k(\overline{q}_{jk}), \xi \right) \right| (\overline{q}_j^{LB} - \overline{q}_{jk}), \quad (20)$$

If we apply simple explicit time integration scheme on Eq. (2) under following CFL condition,

$$\Delta t \frac{L_j}{|T_j|} \left(\sup \left| \frac{dh}{dq} \right| \right) \leq \frac{1}{3}, \quad (21)$$

then two inequality, Eqs. (19)~ (20), can be written as follows.

$$\frac{1}{3}\left(\overline{q}_j^{LB,n} - \max_k(\overline{q}_{jk}) \right) \leq \overline{q}_j^{n+1} - \overline{q}_j^n \leq \frac{1}{3}\left(\overline{q}_j^{LB,n} - \max_k(\overline{q}_{jk}) \right), \quad (22)$$

With the similar algebraic manipulation of the proof of Liu[8], it is shown that the cell-averaged value of n + 1 step is bounded within upper and lower bound of solution cell average values.

$$\overline{q}_j^{LB,n} \leq \overline{q}_j^{n+1} \leq \overline{q}_j^{UB,n}. \quad (23)$$

Thus, the MLP satisfies the maximum principle.

While other limiters on unstructured grids, such as Barth's limiter, LCD and MLG limiter[6, 7, 10], satisfy the maximum principle, the difference can be shown by comparing the stencil of maximum principle (See Fig. 4). Because the allowable distribution of the cell for these limiters depends on Spekreijse's monotonic condition[9], the stencil of these limiters includes cell-averaged values only sharing edge. Thus they have a drawback not to capture multi-dimensional discontinuity accurately. However, MLP condition fully exploits the cell averaged values sharing vertexes, as well as edges, so it is possible to detect on discontinuity, especially near the vertex points.

3.2 MLP condition on unstructured meshes

Implementing MLP condition on the MUSCL-like frameworks, the general formulation of the MLP-u type slope limiter can be written as follows.

$$\phi_{MLP} = \min \begin{cases} \Phi(r_i^{\max}) & if \ \nabla q \cdot \mathbf{r}_{v_i} > 0 \\ \Phi(r_i^{\min}) & if \ \nabla q \cdot \mathbf{r}_{v_i} < 0 \\ 1 & if \ q_i = q_A \end{cases} \quad (24)$$

where $r_i^{\min/\max} = (\hat{q}_{v_i,j}^{\min/\max} - \overline{q}_j)/\nabla q \cdot \mathbf{r}_{v_i}$. The function Φ, called the local limiting function, determines the additional behaviors of limiter by adjusting the magnitude of the slope. For the monotonicity, the value of this function should be less than one.

The immediate form of local limiting function Φ is the upper bound of limiting region. This limiter denotes MLP-u1, which can be written as follows.

$$\Phi(r) = \min(1, r) \quad (25)$$

However, this choice consists of non-differentiable form such as min or max function, which is potential to hamper the convergence of steady state problem. Adapting the Venkatakrishnan's[11] modification for Barth's limiter[10] we also propose MLP-Venkatakrishinan limiter for steady state problem as follow.

$$\Phi\left(\frac{\Delta_+}{\Delta_-}\right) = \frac{1}{\Delta_-} \left[\frac{(\Delta_+^2 + \varepsilon^2)\Delta_- + 2\Delta_-^2 \Delta_+}{\Delta_+^2 + 2\Delta_-^2 + \Delta_+ \Delta_- + \varepsilon^2} \right] \quad (26)$$

where $\varepsilon^2 = (K\Delta x)^3$. The role of value ε is to distinguish the nearly continuous region and discontinuous region, which also prevent clipping problem by similar approach of TVB limiter.

4. NUMERICAL RESULTS

4.1 Shock tube problem

This test is performed to examine the capability of the scheme to resolve discontinuous wave on unstructured grids. The computational domain is[0,1]x[0,0.1] with a triangulation of 101 vertices in the x-direction and 11 vertices in the y-direction. Riemann type initial conditions are considered.

$$(\rho, u, v, p) = \begin{cases} (\rho_L, u_L, v_L, p_L) & \text{if } x \geq 0 \\ (\rho_R, u_R, v_R, p_R) & \text{if } x < 0 \end{cases} \quad (27)$$

Lax Problem:
$$(\rho_L, u_L, v_L, p_L) = (0.445, 0.698, 0, 3.528),$$
$$(\rho_R, u_R, v_R, p_R) = (0.5, 0, 0, 0.571) \quad (28)$$

The y-directional velocity v is zero, and the interface is located at $x = 0.5$. Numerical flux is calculated by RoeM scheme[12]

Fig. 5 shows the density distribution of Lax problem at $t = 0.12$. Comparing to Barth's limiter, MLP-u1 gives much better resolution, except yielding little overshoot near contact discontinuity. The characteristic version of MLP-u1 removes these phenomena.
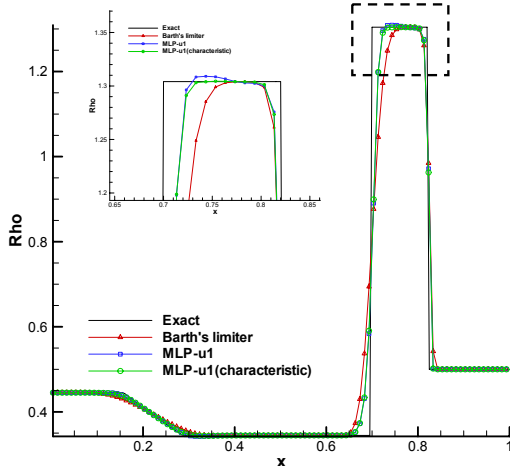
Fig. 5 The comparison density distributions of Lax problem at the centerline.

4.2 Double mach reflection problem

This problem is a very popular test case for high-resolution schemes[13]. The whole computational domain is[0, 4]x[0, 1]. The reflective wall located at the bottom of computational domain beginning at $x = 1/6$. At first, a right-moving shock $M = 10$ is positioned at $(x = 1/6, y = 0)$ making 60 ° angle with respect to the x-axis. Lax-Friedrichs scheme is used as a numerical flux and the computation was carried out until $t = 0.2$

Fig. 6 shows the comparison of density contours using triangular grids whose size h is $1/480$. Both limiters give monotone solutions, but MLP-u1 limiter gives a much enhanced resolution for shock discontinuity and the complicated flow structure below the Mach stem than Barth's limiter.

4.3 Isentropic vortex problem

Since vortex flow is a purely multi-dimensional phenomenon, it is a good test case to examine the accuracy of a numerical scheme in multiple dimensions flow without shock waves and turbulence. Since the flowfield is inviscid, the exact solution is just a passive advection of the initial vortex with mean flow. The mean flow, which is considered as a free stream, is $\rho_\infty = 1$, $p\infty = 1$ and $(u_\infty, v_\infty) = (0,0)$. The perturbation values for the isentropic vortex are given by

$$(\delta u, \delta v) = \frac{\varepsilon}{2\pi} e^{0.5(1-r^2)} (-\bar{y}, \bar{x}), \quad \delta T = -\frac{(\gamma-1)\varepsilon^2}{8\gamma\pi^2} e^{1-r^2}, \quad (29)$$

The strength of vortex is $\varepsilon = 5$. Here, $(\bar{x}, \bar{y}) = (x - x_0, y - y_0)$, where (x_0, y_0) are the coordinate of the center of initial vortex, and $r^2 = \bar{x}^2 + \bar{y}^2$. From $\rho = \rho_\infty + \delta\rho$, $u = u_\infty + \delta u$, $v = v_\infty + \delta v$, $T = T_\infty + \delta T$ and isentropic relation, the conservative variable of a state is given by

$$\rho = T^{1/(\gamma-1)} = \left[1 - \frac{(\gamma-1)\varepsilon^2}{8\gamma\pi} e^{1-r^2}\right]^{1/(\gamma-1)}, \quad (30)$$
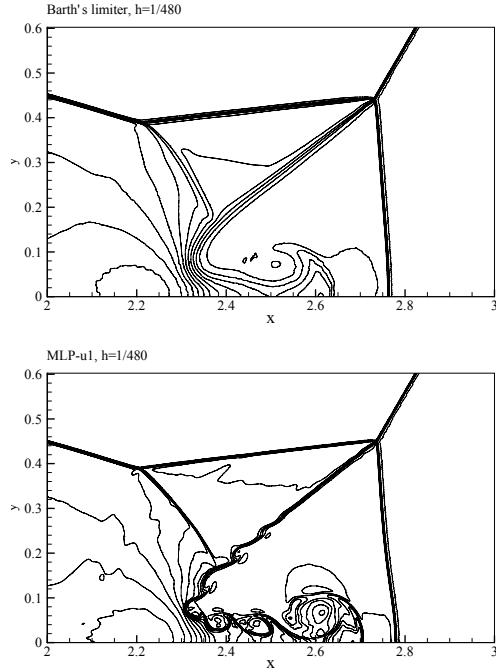

Fig. 6 Density contours at blown-up region around the double Mach stems. (Top: Barth's limiter, Bottom: MLP-u1)

$$\rho u = \rho(u_\infty + \delta u) = \rho\left[1 - \frac{\varepsilon}{2\pi} e^{0.5(1-r^2)}\bar{y}\right], \quad (31)$$

$$\rho v = \rho(v_\infty + \delta v) = \rho\left[1 + \frac{\varepsilon}{2\pi} e^{0.5(1-r^2)}\bar{x}\right], \quad (32)$$

$$p = \rho^\gamma, \quad (33)$$

$$e_t = \frac{p}{\rho(\gamma-1)} + \frac{1}{2}(u^2 + v^2). \quad (34)$$

The computational domain is $-5 \leq x \leq 5$ and $-5 \leq y \leq 5$ and periodic boundary condition is applied. The triangular mesh is created by dividing uniform square elements along the diagonal. Roe's FDS[14] is applied as a numerical flux.

Fig. 7 shows the density contours of Barth's limiter and proposed limiter. Due to the large dissipation of Barth's limiter, the contour of vortex is smeared and distorted. On the other hand, MLP-u1 limiter can keep vortex shape.

Fig. 8 shows the comparison of density distributions at the vortex center line. Similar to a previous figure, it clearly shows the low-dissipative characteristic of proposed limiting strategy.

Table 1 presents the analysis of the order of accuracy at time t = 1. Comparing the result of Barth's limiter, MLP-u1 limiter maintains higher order accuracy.

4.4 Double shock reflection

In order to investigate the convergence characteristic of steady state flow, this test is considered. The flow of Mach 2 blows to the pipe of which deflection angle is 15 degree. The mesh is consisted with 6194 triangular elements.
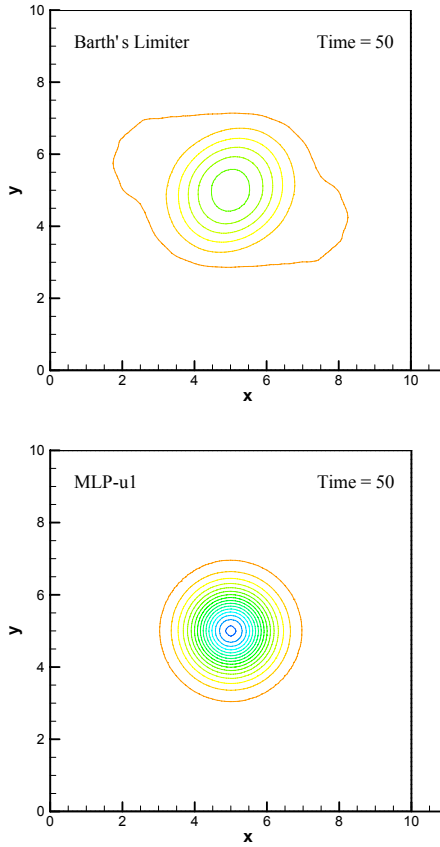
Fig. 7 Density contours of evolution of vortex at $t = 50$. (Top: Barth's limiter, Bottom: MLP-u1)
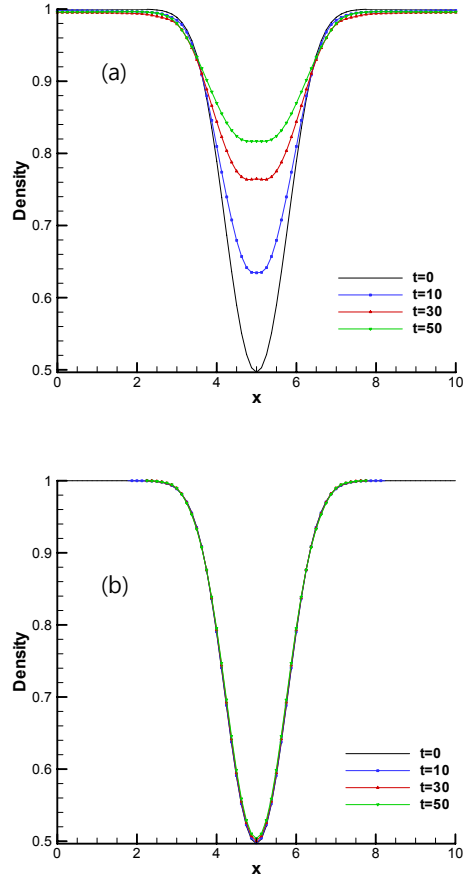

Fig. 8 Density distributions of the evolution of vortex along the center line. (Top: Barth's limiter, Bottom: MLP-u1)

Table 1 Grid refinement test for the evolution of isentropic vortex at $t = 2.0$

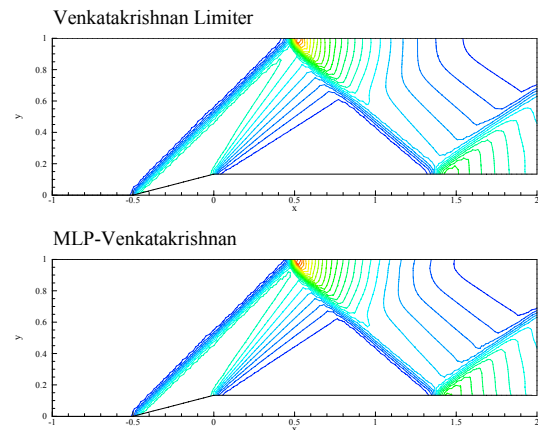|		L_∞	Order	L_1	Order
Barth	10x10x2	2.08E-1	-	1.13E-2	-
	20x20x2	1.19E-1	0.81	4.73E-3	1.26
	40x40x2	5.98E-2	1.00	2.19E-3	1.13
	80x80x2	3.20E-2	0.90	1.07E-1	1.01
MLP-u1	10x10x2	1.72E-1	-	9.59E-3	-
	20x20x2	4.16E-2	2.05	2.05E-3	1.94
	40x40x2	8..62E-3	2.27	5.87E-4	2.09
	80x80x2	1.58E-3	2.44	1.29E-4	2.19
MLP-Venkata krishnan	10x10x2	1.87E-1	-	1.04E-2	-
	20x20x2	5.78E-2	1.69	2.81E-3	1.89
	40x40x2	1.19E-2	2.28	6.59E-4	2.09
	80x80x2	2.04E-3	2.55	1.43E-4	2.20
Without Limiter	10x10x2	1.48E-1	-	9.77E-3	-
	20x20x2	3.97E-2	1.90	2.50E-3	1.96
	40x40x2	7.73E-3	2.36	5.62E-4	2.16
	80x80x2	1.54E-3	2.32	1.24E-4	2.19

Fig. 9 Comparison of pressure contours for double shock reflection. (Top: Venkatakrishnan limiter, Bottom: MLP-Venkatakrishnan)
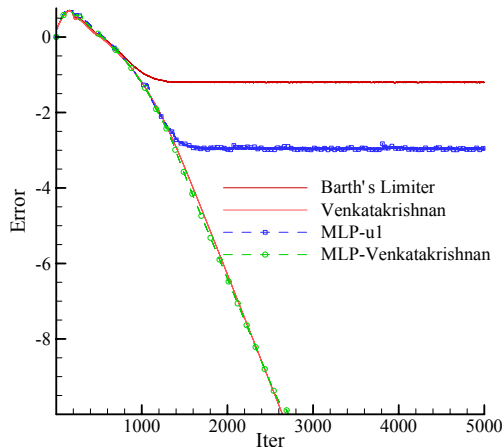
Fig. 10 Error history of double shock reflection.

Fig. 9 is the comparison of pressure distributions of Venkatakrishnan limiter and MLP-Venkatakrishnan limiter. The value K of ε set to 0.1. Though they show little difference of pressure contour, both limiters give a monotone solution.

Fig. 10 shows convergence history of each limiter. While the limiters that contain non-differentiable function, such as min or max, fails to converge to machine level order, the result of Venkatakrishnan limiter and MLP-Venkatakrishnan limiter shows good convergence characteristics.

4.5 Viscous shock tube problem

This test case shows the complex viscous flow structure involving the interaction with shock wave, boundary layer and vortex. As diaphragm is broken, the boundary layer grows by viscosity at the horizontal wall. After the shock wave reaches the vertical wall, this wave interacts with boundary layer, which makes complex flow with λ-shape shock and vortices.

For the two dimensional case, Daru and Tenaud proposed this configuration[15]. The size of shock tube is *1* length and *1* height and diaphragm is located at *x = 0.5*. The initial state of both chambers is given as follows.

$$\begin{aligned}(\rho_L, u_L, v_L, p_L) &= (120, 0, 0.120/\gamma), \\ (\rho_R, u_R, v_R, p_R) &= (1.2, 0, 0, 1.2/\gamma)\end{aligned} \quad (35)$$

The Reynolds number is 200 and Prandtl number is 0.13. With AUSMPW+ inviscid flux[16], the viscous flux is calculated by Frink's approach[17]. TVD Runge-kutta 3rd order time integration method is used with CFL = *0.5*.

On Fig. 11, the density contours are compared at *t = 1*. The result of MLP-u1 limiter on coarse grid is similar to that of Barth's limiter on fine grid, which has about four times more triangular elements. Also, the vortexes in the boundary layer of Barth's limiter lose it shape due to the excessive diffusion. On the other hand, the vortexes of MLP-u1 limiter is captured maintaining significantly better accuracy.

Fig. 12 shows the density distributions on the bottom wall. Investigating around the primary vortex region, it is shown the diffusive behavior of Barth's limiter.

Table 2 is the comparison of the primary vortex size. Comparing to the result of structured grid[4], the result of MLP-u1 limiter on fine grid is almost the same with the converged value of MLP on structured grid. The size of Barth's limiter on fine grid is even smaller than that of
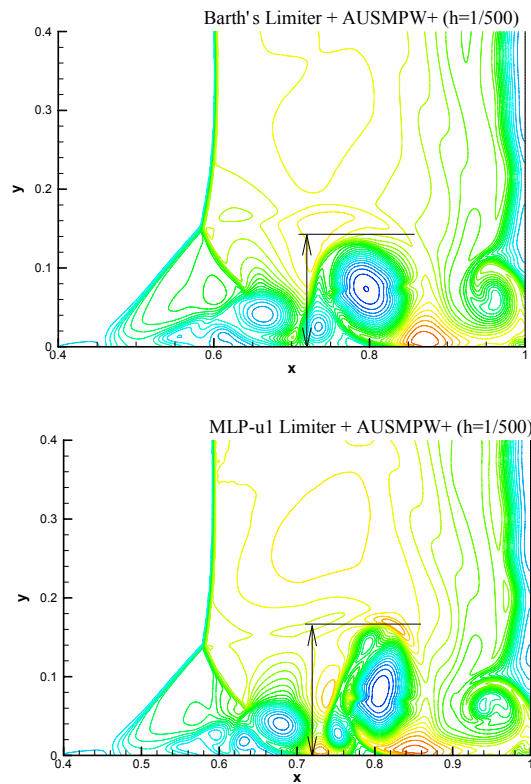

Fig. 11 Comparison of density contours for viscous shock tube. problem (Top: Barth's limiter, Bottom: MLP-u1)
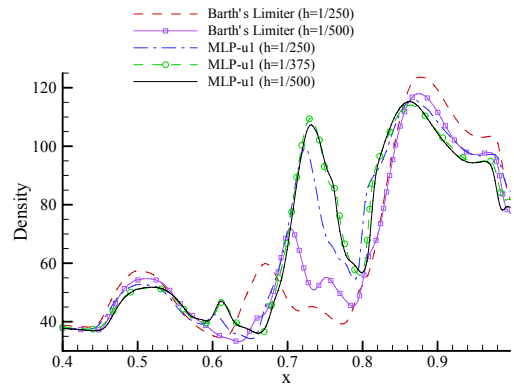

Fig. 12 Comparison of density distributions along the wall.

MLP-u1 limiter on coarse grid. From the above comparison, the MLP-u limiter resolves the complex viscous flow pattern accurately.

Table 2 Size of primary vortex for viscous shock tube problem.

	Barth's limiter	MLP-u1
$h = 1/250$	0.124	0.147
$h = 1/350$	0.135	0.161
$h = 1/500$	0.142	0.168

5. CONCLUSIONS

With the previous successful results of MLP on structured grids, the new limiting process, called MLP-u, is proposed on unstructured grids. The key idea of MLP-u is the extension of MLP condition, which is the essential part of ensuring monotonicity on structured meshes. With this condition, the values at the vertex, where an extreme of the linearly distributed cell is occurred, are properly restricted based on the distribution of neighboring cells. The satisfaction of maximum principle also guarantees the monotonicity of the solution. On the MUSCL-type framework, the MLP-u type slope limiters are proposed.

The various numerical tests clearly show the desirable characteristics of proposed limiting strategy. Maintaining the multi-dimensional monotonicity and robustness, the accuracy is significantly improved on capturing the complex flow structured.

REFERENCES

[1] 1983, Harten, A., "High Resolution Schemes for Hyperbolic Conservation Laws," *J. Comput. Phy*s., Vol.49, pp.357-393.

[2] 1984, Sweby, P.K., "High Resolution Schemes Using Flux Limiters for Hyperbolic Conservation Laws," *SIAM J. Num. Anal.*, Vol.21, pp.995-1101.

[3] 1985, Goodman, J. B. and Leveque, R.J., "On the Accuracy of Stable Schemes for 2D Scalar Conservation Laws," *Math. Comput.*, Vol. 45, pp.15-21.

[4] 2005, Kim, K.H. and Kim, C., "Accurate, Efficient and Monotonic Numerical Methods for Multi-dimensional Compressible Flows Part II: Multi-dimensional Limiting Process," *J. Comput. Phys.*, Vol.208, pp.570-615.

[5] 2008, Yoon, S-.H., Kim, C. and Kim, K.H., "Multi-dimensional Limiting Process for Three dimensional Flow Physics Analyses," *J. Comput. Phys.*, Vol.227, pp.6001-6043.

[6] 1996, Batten, P., Lambart, C. and Causon, D. M., "Positively conservative high resolution convection schemes for unstructured elements," *Int. J. Num. Eng.*, Vol.39, pp.1821-1838.

[7] 1999, Hubbard, M.E., "Multidimensional slope limiters for MUSCL-type finite volume schemes on unstructured grids," *J. Comput. Phys.*, Vol.155, pp.54-74.

[8] 1993, Liu, X.D., "A Maximum Principle Satisfying Modification of Triangle Based Adaptive Stencils For the Solution of Scalar Hyperbolic Conservation Laws," *SIAM J. Num. Anal.*, Vol.30, pp.701-716.

[9] 1987, Spekreijse, S., "Multigrid Solution of Monotone Second-order Discretizations of Hyperbolic Conservation Laws," *Math. Comp.*, Vol.49, pp.135-155

[10] 1989, Barth, T.J. and Jespersen, D., "The design and application of upwind scheme on unstructured meshes," *Proc.27AIAA-RENO*, AIAA 89-0366

[11] 1995, Venkatakrishnan, V., "Convergence to Steady State Solutions of the Euler Equations on Unstructured Grids with Limiters," *J. Comput. Phys.*, Vol.118, pp.120-130.

[12] 2003, Kim, S., Kim, C., Rho, O.H. and Hong, S.K., "Cures for the Shock Instability: Development of a Shock-stable Roe Scheme," *J. Comput. Phys.*, Vol.185, pp.342-374.

[13] 1984, Woodward, P. and Colella, P., "The Numerical Simulation of Two-dimensional Fluid Flow with Strong Shocks," *J. Comput. Phys.*, Vol.54, pp.115-173.

[14] 1981, Roe, P.L., "Approximate Riemann Solvers, Parameter vectors and Difference Schemes," *J. Comput. Phys.*, Vol.43, pp.357-372.

[15] 2001, Daru, V. and Tenaud, C., "Evaluation of TVD High Resolution Schemes for Unsteady viscous Shocked flows," *Comput. Fluids*, Vol.30, pp.89-113

[16] 2001, Kim, K.H., Kim, C., and Rho, O.H., "Methods for the Accurate Computations of Hypersonic Flows, Parts I: AUSMPW+ Schemes," *J. Comput. Phys.*, Vol.174, pp.38-80.

[17] 1991, Frink, N.T., "Upwind Schemes for Solving Euler Equations on Unstructured Tetrahedral Meshes," *AIAA J.*, Vol.30, pp.70-77.

Unstructured Quadrilateral Surface Grid Generation and Cell Size Control

Byoungsoo Kim*

* Department of Aerospace Engineering, Chungnam National University, Daejeon, Korea
(Tel : +82-42-821-6686; E-mail: kbskbs@cnu.ac.kr)

Abstract: In this paper grid generation of unstructured quadrilateral surface grids is described. The current approach uses conventional Advancing Front Method which is used to generate unstructured triangular grids. Grid cell size control is done by using closeness-based global interpolation method controlled by pre-described control elements. Algorithm and procedure for quadrilateral grid generation using AFM method and cell size control method are described. Examples of quadrilateral grid generation are shown, and difficulties and problems related to the current approach are also discussed.

Keywords: CFD, FEM, Unstructured Quadrilateral Grids, Advancing Front Method, Hybrid Grid System.

1. INTRODUCTION

Numerical problem solving techniques such as CFD and FEM method are being widely used in various fields of engineering such as fluid mechanics and structural analysis. These techniques can be categorized into finite difference method, finite volume method, and finite element method, and others. Each of these numerical techniques eventually solves a set of algebraic equations which are obtained by approximately applying the governing partial differential equations on a set of simpler shaped cells which replace the whole domain of interest including boundaries.

It is well-known that the quality and the number of those cells have strong influence on the convergence and accuracy of solutions obtained by those numerical techniques, and furthermore grid generation is usually considered as a bottleneck for a routine application of numerical techniques in the engineering process because of its labor-intensive and error-prone nature. The grid system can be categorized into two types: structured grids and unstructured grids. The structured grid system is characterized by its orderly fashion of node connectivity among neighboring nodes, while the unstructured grids don't require any orderliness of node connectivity. Generating structured quadrilateral meshes for general 2-D region and structured hexahedral meshes for 3-D region usually requires user's experience and labor due to its requirement for orderliness of node distribution, while unstructured grids with triangular cells(2-D) or tetrahedral cells(3-D) can be much easily generated even for very complex domains due to its favorable flexibility nature of node connectivity.

On the other hand the shape of grid cell has strong influence on the accuracy and the cost of numerical analysis. Quadrilateral cells(2-D) or hexahedrons(3-D) have several desirable properties compared to the triangles(2-D) or tetrahedrons(3-D). Blacker summarized those properties and those are quoted as follows:[1]

- Hexahedron provides shape functions with additional terms that may increase the accuracy of the solution
- Hexahedron provides directional sizing without losing accuracy. For example, a very thin hexahedron within a boundary layer for fluid flow calculations performs far better than thin tetrahedron.
- A conformal mesh provides the most accurate form of connectivity within the region. Non-conformal interfaces may decrease the meshing complexity but increase the error, at least locally.
- A hexahedra mesh decreases the overall element count. A tetrahedral mesh usually increases the element count 4 to 10 fold over a hexahedral mesh.

In author's lab a research to develop a computer program which allows an automatic grid generation of unstructured grids for general 3-D regions is in progress, and robust surface grid generation method for general-shaped boundary surfaces is required to generate hybrid grids consisting of unstructured triangles and quadrilaterals. This paper describes how surface grid generation of unstructured quadrilateral grids can be accomplished by applying Advancing Front Method(AFM) which are conventionally used to generate triangular cells[2].

2. UNSTRUCTURED GRIDS

In CFD research field structured multi-block grids have been traditionally the grid topology of more preference in the past compared to the unstructured grids in the structural research area using FEM methodology. Trend is, however, shifting, and unstructured tetrahedral grids are being adopted more widely in the CFD area also due to its relative advantageous features compared to structured approach including flexibility and robustness of grid generation even for very realistic and complicated geometries. The case of Fluent could be example of that kind of trend. This one of major commercial CFD software has changed its underlying grid system from traditional structured grid based approach to unstructured grid based one[3]. Even though structured grid system has its own advantages and strengths, one of major drawbacks of structured grid approach is the requirement of experience and trial-and-error in the grid generation stage while unstructured grid system can be relatively easily constructed.

In recent years many researchers and CFD software users are using unstructured grids to calculate flow fields for very complicated geometries, such as aircrafts with enough details considered. It can be said that due to its major advantage of flexibility, tetrahedral grids are used most often among various grid types in the 3-dimensional unstructured grid approach. For the accurate calculation of flow fields by the flow solvers the grid system should have good quality regardless of grid types. For the case of generating 3-dimensional tetrahedral grids, triangular surface grid generation is required, and the triangular cells can have its best possible quality when they are equilateral. Even though there are other measures for grid quality evaluation such as grid size gradient, grid quality is most influenced by the angular skewness which is directly affected by how much the shape deviates from the equilateral shape for the case of triangles. This is why relatively many triangular cells are distributed near the leading edge of a wing in spite of low flow gradient in the span-wise direction compare to the chord-wise direction, as shown in Fig. 1(a). By using stretched(or anisotropic) triangular cells it is possible to use less number of cells, but the deterioration of flow solution